J Porous Mater (2018) 25:747–759
DOI 10.1007/s10934-017-0488-9

# Pt/Ni wet impregnated over Al incorporated mesoporous silicates: a highly efficient catalyst for anisole hydrodeoxygenation

**Pichaikaran Sudhakar**[1] · **Arumugam Pandurangan**[1]

Published online: 9 August 2017


**Abstract** This work reports, formation of benzene from anisole via hydrodeoxygenation process using vapour phase fixed bed reactor. The surface properties of bimetallic catalysts such as textural properties, acidic, and Pt/Ni dispersion has established by various characterization techniques. The reaction was carried out at 370 and 420 °C with space velocity 3.3 & 6.6 $h^{-1}$, over acidic and non-acidic supported mono and bimetallic catalysts. The optimum conversion and selectivity was observed at 420 °C and WHSV = 3.3 $h^{-1}$ for all mono and bimetallic catalysts. Pt/Ni/Al-SBA-15 acidic bimetallic catalyst shows maximum anisole conversion 59% with benzene selectivity 37% under atmospheric pressure, due to the more acidic centres and high dispersion of Pt/Ni species on the bimetallic catalyst, enhance the anisole conversion; this was proved by $NH_3$-TPD and HR-TEM analysis. The acidic Pt/Ni bimetallic catalyst shows higher anisole conversion as compared to the mono metallic Pt/Ni catalysts and it works predominantly through demethylation and hydrogenolysis reaction pathway.

**Keywords** Anisole · Pt/Ni bimetal · Al-SBA-15 · Hydrodeoxygenation · Benzene

## 1 Introduction

In recent years, much attention is paid on bio-fuels, because they reduce serious environmental pollution associated with the uses of fossil fuels [1–3]. Many researchers have focussed interest towards the conversion of biomass as it is an important renewable resources for fuels, fuel additives and value added chemicals [4]. Among the various forms of biomass, lignin is one of the most attracted bio-mass due to its higher aromatic content of bio based atom economy. However, the direct use of bio oil from lignin is not feasible due to its high oxygen content and instability. Better quality of bio-fuel could be obtained by the removal of oxygen from its bio-oil. Various catalytic processes have been extensively studied for oxygen removal, for instance, catalytic cracking, reduction and oxidation for upgrading the quality of bio fuel. Unfortunately, these processes generate high volatile gaseous products. Among, the various catalytic processes, hydrodeoxygenation has been extensively studied and is considered to be interesting for upgrading aromatics and liquid alkanes with effective routes [5–7]. Major source of lignin bio-oil containing methoxy–phenyl group, viz., anisole is considered as the model compound for the production of bio-fuel. It has added advantages of being liquid at room temperature, ease of handling for reaction as well as analysis [8]. The formal HDO catalyst such as sulfided CoMo/ $Al_2O_3$ and NiMo/ $Al_2O_3$ have been most commonly used catalysts in HDO reaction. More over this type of catalysts show faster deactivation by coke formation due to the production of high sulphur streams [9].Therefore, designing a suitable catalyst without much deactivation and with most feasible condition for producing high yield of liquid fuels from pyrolysis of bio-oil is a major challenge. In this aspect, metal supported catalysts play a significant role in HDO reactions. Particularly, bimetallic catalysts possessing synergistic effect due to the presence of metallic and acidic sites may probably be utilized during the HDO reaction pathway. The metal sites are used to activate molecular hydrogen where as acid sites are used to activate oxy group of reactant [10].

✉ Arumugam Pandurangan
pandurangan_a@yahoo.com

[1] Department of Chemistry, Anna University, Chennai 600 025, India

An increasing attention was focussed on oxide supported catalyst, particularly on silica material, which was used as catalytic material due their practical utilization. In particular mesoporous SBA-15 has sought great interest in catalysis due to their ordered channels with large pore size, higher wall thickness than other supports [11]. In the field of biomass research, especially in the conversion of lignin model compound into fuels and value added chemicals, SBA-15 has been paid much attention because it provides higher surface area, limiting micro pore volume and has greater wall thickness to offer greater thermal stability to supported metal catalyst. Due to these reasons, supported metal catalysts play a significant role in biomass conversion for obtaining better activity and selectivity through different catalytic pathways involved during the HDO reactions [12].

In this investigation, Pt/SBA-15, Ni/SBA-15, Pt/Ni/SBA-15 and Pt/Ni/Al-SBA-15 mono and bimetallic catalysts were prepared using wet-impregnation method and investigated for their catalytic efficiency over hydrodeoxygenation of anisole under two different temperatures and two different space velocities with atmospheric pressure. The crystalline phase identification of active metal, morphology of the support and textural properties were studied. The surface metal–acid function present on the bimetallic catalyst was crucial in determining catalytic behaviour, and they have been reported to facilitate the hydrogenolysis of anisole and transmethylation reactions [13–15]. Based on these studies the correlations between surface characteristics and catalytic activity were further investigated for HDO of anisole.

## 2 Experimental

### 2.1 Chemicals

All chemicals with AR grade purity (analytical reagent grade) were purchased and used as received without further purification. Tetraethylorthosilicate (TEOS; Aldrich) was used as silica source, Triblockcopolymer (Pluronic P123, triblock Poly (ethylene oxide)–Poly (propylene oxide)–Poly (ethylene oxide) ($EO_{20}$ $PO_{70}$ $EO_{20}$); Aldrich: M.W.5800) were used as template (>98% pure). Hydrochloric acid (35%) used in the synthesis was purchased from SRL Biochem (India) Ltd. Anisole was purchased from SRL Biochem (India) Ltd. (99% pure). Nickel (II) nitrate hexahydrate (Aldrich) and chloroplatinic acid hexahydrate (SRL Biochem India Ltd) were used as active metal sources. 99% pure hydrogen was purchased from Indo gas (India) Ltd.

### 2.2 Catalysts preparation

According to the literature, Si-SBA-15 and Al-SBA-15 support were synthesised via direct hydrothermal method [16]. The aluminium containing SBA-15 mesoporous material was synthesised as follows: 4 g of Pluronic (P123) was added to 30 mL of deionised water in a polypropylene bottle. The contents were stirred for 4 h and a clear solution was obtained. 70 g of 0.28 M hydrochloric acid was added and stirring was continued for another 2 h. Subsequently, 9 g of TEOS and the calculated amount of aluminium iso propoxide were added to the solution to obtain a given Si/Al ratio (25). The resulting mixture was stirred for another 24 h at 40 °C and aged at 100 °C for 48 h. The obtained solid material was recovered by filtration, washed with several times with distilled water and dried overnight at 100 °C. Finally, the material was calcined at 550 °C in air for 6 h. Same procedure was followed for synthesis of Si-SBA-15. The active metal containing 1.0% Pt/SBA-15, 7.0% Ni/SBA-15, 1.0% Pt/7.0% Ni/SBA-15 and 1.0% Pt/7.0% Ni/Al-SBA-15(25) material were prepared by wet-impregnation method. 1 g of synthesised Si-SBA-15 and Al-SBA-15(25) were transferred separately to 50 mL round bottom flask and added 25 mL of deionised water and stirred for 15 min. A homogeneous mixture was obtained. The required wt% of metal sources was dissolved in 5 mL of deionised water and added drop by drop into the mixture. After stirring for 6 h, water was removed by evaporation and dried at 100 °C for 12 h and calcined in atmospheric air at 400 °C for 6 h.

### 2.3 Characterization of supports and catalysts

X-ray diffraction (XRD) patterns of the prepared materials were recorded by PAN Analytical diffractometer using Nickel filter Cu Kα radiation (λ= 1.5406 Å). The crystalline phase was identified by matching the peaks appearing in the XRD line of the test sample with JCPDS (joint committee on powder diffraction standards) data files and the metal crystallite size was calculated by the Scherrer equation. The porous nature of the materials was measured by nitrogen adsorption–desorption experiment at 77 K using Quanta chrome 2010-09. Surface area was calculated by the B.E.T. equation. Pore volume and pore size distribution were measured by BJH (Barrett–Joyner–Halenda) method using the adsorption branch of the isotherm. XPS measurements was handled using Omicron Nanotechnology, GmBH, Germany XM1000 monochromated with Al $K_\alpha$ radiation of 1483 eV operated at 300 W (20 mA emission current, 15 kV) and a base pressure in the analysis chamber higher than $5 \times 10^{-5}$ mbar. The survey spectrum was performed with a step size of 0.5 eV along with 50 eV as the pass energy. Collected XPS spectra were processed by CasaXPS software v.2.2.84. The complete reduction profile of prepared materials was measured by ($H_2$-TPR) hydrogen temperature programmed reduction using Quanta chrome 2010. About 100 mg of the dried sample was loaded in a thermostatic zone. The TPR profiles were obtained by the sample which was pre-treated

at 115 °C in highly pure helium gas (25 cc $min^{-1}$) for 1 h and cooled to room temperature and then the gas was changed to mixture of 5 vol% $H_2$/Ar (25 cc $min^{-1}$) introduced into the sample tube at room temperature till baseline is stable. Then TPR started from room temperature to 800 °C with heating rate 10 °C $min^{-1}$. The hydrogen consumption was determined by calibration and further integration of the output signal from thermal conductivity detector (TCD). The acidity of materials was measured by temperature programmed desorption of ammonia $NH_3$-TPD using the same setup as in the $H_2$-TPR analysis. The procedure followed for the TPD measurements involved the pre-treatment of the catalyst by flow of helium at 500 °C for 1 h and cooling to 100 °C. The mixture of 10 vol% $NH_3$/He was introduced and physically adsorbed $NH_3$ was removed by purging with a helium flow at 100 °C until the base line was flat. Thereafter, the chemisorbed ammonia was desorbed by increasing the temperature up to 500 °C with a rate of 10 °C $min^{-1}$, its concentration in the effluent stream being monitored by a TCD signal. Metal contents were determined by using an inductively coupled plasma-optical emission spectrometer (ICP-OES) Perkin Elmer Optima 5300Dv instrument. TGA of the spent catalysts were performed using a waters TA instrument SDTQ 600 analyser. 10 mg of the sample was heated from 85 to 900 °C with heating rate 20 °C $min^{-1}$ in air atmosphere. The HR-TEM images were obtained on a TECNAI T30 $G^2$ FEI company and working at accelerating voltage of 300 kV. The samples for the HR-TEM study were prepared by ultrasonic dispersion in acetone for 1 h and consequent deposition of the suspension on a copper grid and dried at 37 °C for 15 min and examined under HR-TEM.

### 2.4 Reaction procedure

The catalytic reaction was carried out in a fixed-bed reactor using quartz tube. Pt/SBA-15, Ni/SBA-15 mono metal and Pt/Ni-SBA-15, Pt/Ni/Al-SBA-15 bimetal catalysts were used for hydrodeoxygenation of anisole. The anisole reactant flow was fed into the reactor using syringe infusion pump (Ravel Hiteks, India). 0.3 g of mono metallic or bimetallic catalyst was placed in the reactor tube and supported on either side with thin layer of quarts wool and ceramic beds. The reactor was heated to reaction temperature with the help of a tubular furnace controlled by a digital temperature controller. The bottom of the quartz tube was connected to a coiled condenser and a receiver to collect the reaction products. Before reaction, the catalyst was reduced in the reactor with flow of hydrogen 50 mL $min^{-1}$ at 500 °C. During the catalytic reaction, the hydrogen flow rate was 50 mL $min^{-1}$ and anisole was fed at a rate of 1 mL $h^{-1}$ or 2 mL $h^{-1}$ corresponding to a space velocity of 3.3 $h^{-1}$ and 6.6 $h^{-1}$ respectively. The reaction was studied at 370 and 420 °C under atmospheric pressure. Liquid samples collected at 1 h intervals were analysed by off-line gas chromatograph (GC-17A Shimadzu) equipped with a Flame ionization detector and Rtx-5 (30.0 m × 0.25 mm, 0.25 µm film thickness) column for product analysis. The conversion and selectivity of anisole was calculated from the area % of reactant and product by the gas chromatography analysis.

## 3 Results and discussion

### 3.1 Characterization of catalysts

#### *3.1.1 Powder XRD analysis*

Figure 1a shows the low angle XRD pattern of support and active metal supported catalysts. The low angle XRD pattern of Si-SBA-15 shows three well-resolved peaks with crystalline plane (100), (110), and (200) indicating that the materials are 2D hexagonal mesostructured with space group *p6mm* symmetry [17]. A similar trend was observed for the material consisting of platinum and nickel containing mono and bimetal catalysts. The intensity of platinum and nickel promoted catalysts was slightly decreased as compared to pure material and further small peak shift was observed at higher diffraction angle and these changes could not affect the structures of catalyst as compared with Si-SBA-15. The unit cell parameter $a_o$ of calcined samples was calculated, as shown in Table 1. The results have been in agreement with reported literature and suggest that mesoporous silica SBA-15 structure was retained even after metal loading [18]. Figure 1b showed wide angle XRD patterns of Pt/SBA-15, Ni/SBA-15, Pt/Ni/SBA-15, Pt/Ni/Al-SBA-15 catalysts in the region of $2\theta = 30°–80°$. The nickel supported mono and bimetallic catalysts shows NiO cubic phase at $2\theta = 43°$, 62° and 71° with (111), (200) and (220) planes [19]. The intensity of cubic NiO phase was high in mono metallic catalyst Ni/SBA-15, while in the bimetallic catalysts the intensity of this phase decreased, indicating that the addition of platinum with its high dispersion in the silica matrix decreases the NiO crystallite phase. The three new diffraction peaks appeared at $2\theta = 39.78°$, 46.28° and 67.48° were assigned to (111), (200) and (220) reflections of face-cantered cubic (fcc) platinum were in good agreement with JCPDS card (No. 04-0802) [18]. The particle size of platinum for mono and bimetallic catalyst was estimated from the (111) peaks as given in Table 1. The intensity of the corresponding reflections was much lower in case of bimetallic catalyst than that of the mono metallic catalyst, suggesting that most of the platinum in the bimetallic catalysts should be highly dispersed on the catalyst surface.

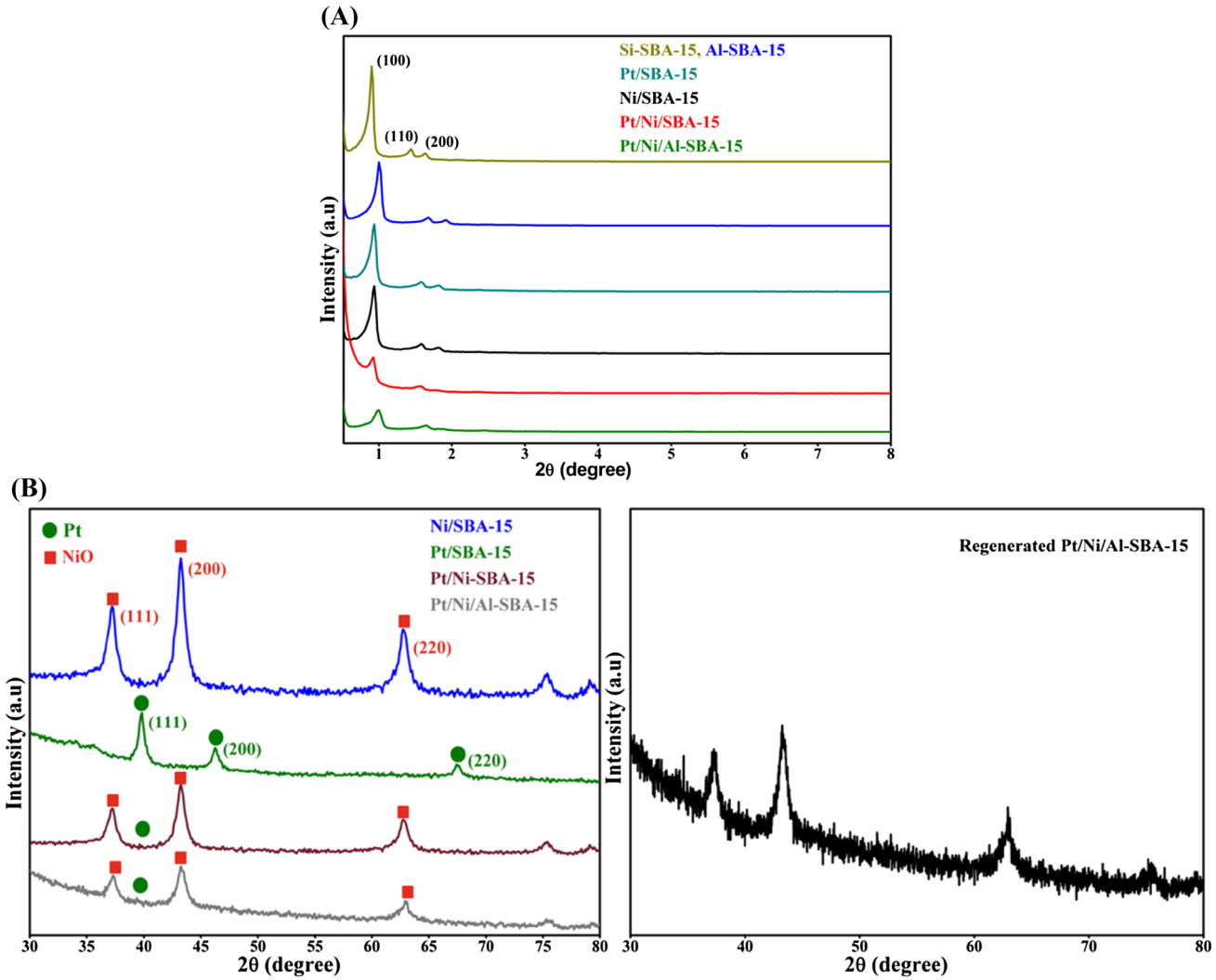


**Fig. 1** **a** Low angle XRD patterns of calcined Si-SBA-15, Al-SBA-15 support and Ni/SBA-15, Pt/SBA-15, Pt/Ni/SBA-15 and Pt/Ni/Al-SBA-15 catalysts. **b** High angle XRD patterns of Ni/SBA-15, Pt/SBA-15, Pt/Ni/SBA-15, Pt/Ni/Al-SBA-15 and Pt/Ni/Al-SBA-15 regenerated catalysts

### *3.1.2 $N_2$ sorption analysis*

Nitrogen adsorption–desorption isotherms and pore size distribution of the supports and the catalysts are shown in Fig. 2a, b. All the samples obtained are type IV isotherms with a broad H1hysteresis loops, indicating formation of mesopores with 2D-hexaganol structure [17]. The BJH pore size distribution curves are narrow and centred around 11.0 nm for Si-SBA-15. Further, incorporation of Al into Si-SBA-15 matrix, the pore size distribution becomes slightly wider, and average pore size shifts to 11.3 nm, indicating that the pore structure is slightly increased by the introduction of aluminium. It confirmed that most of the aluminium species are successfully incorporated into the framework of Si-SBA-15 support [8]. Moreover, the shape of $N_2$ adsorption desorption isotherms of platinum and nickel supported catalyst was similar to that of the original support, suggesting that the mesoporous structure of Si-SBA-15 was intact upon platinum and nickel impregnation. In fact, the mean pore diameter of mono metallic platinum and nickel catalyst was 9.4 nm and it decreased to about 6.1 nm and 6.0 nm for platinum and nickel supported bimetallic catalysts. The BET surface area ranges from 474 to 885 $m^2\ g^{-1}$ with pore volume in the range of 0.85–1.3 cc $g^{-1}$ are tabulated in Table 1. Both surface area and the total pore volume decreased after the impregnation of platinum and nickel on bimetallic catalysts. This might have been caused due to the partial pore blockage of the support by platinum and nickel oxide particles [20].

### *3.1.3 X-ray photoelectron spectroscopy*

XPS studied the chemical state of Pt and Ni on Pt/Ni/Al-SBA-15 bimetallic catalysts, and the results are shown in

**Table 1** Textural properties, surface acidity and crystallite size of Si-SBA-15, Al-SBA-15 support and Pt/Ni supported mono and bimetallic catalysts

| Sample | Metal content[a] (%) | | $a_0$ (nm) | $S_{BET}$[b] ($m^2\ g^{-1}$) | $V_{total}$[c] (cc $g^{-1}$) | $P_D$[d] (nm) | $P_W$[e] (nm) | Total acidity[f] (mmol $g^{-1}$) | Metal crystallite size[g] (nm) | |
|---|---|---|---|---|---|---|---|---|---|---|
| | Ni | Pt | | | | | | | Ni | Pt |
| Si-SBA15 | – | – | 14.9 | 850 | 1.28 | 11.0 | 3.9 | – | – | – |
| Al-SBA15(25) [55 h] | – | – | 15.6 | 885 | 1.30 | 11.2 | 4.4 | 0.24 | – | – |
| Pt/SBA-15 | – | 0.97 | 11.8 | 620 | 1.00 | 9.4 | 2.4 | 0.01 | – | 12 |
| Ni/SBA-15 | 6.85 | – | 11.6 | 574 | 0.88 | 9.3 | 2.3 | 0.01 | 18 | – |
| Pt/Ni/SBA-15 | 6.34 | 0.92 | 9.3 | 483 | 0.85 | 6.3 | 3.0 | 0.02 | 21 | 14 |
| Pt/Ni/Al-SBA-15 | 6.55[(6.02)i] | 0.95[(0.87)i] | 9.2 | 474 | 0.85 | 6.1 | 3.1 | 0.18 | 19[(21)j] | 15[(16)j] |

[a]Actual metal content from ICP-OES analysis

[b]BET Surface area calculated from the adsorption branch of the $N_2$ isotherm

[c]Total Pore volume calculated from the adsorption branch of $N_2$ isotherm

[d]Average mesopore diameter calculated from the adsorption branch using the BJH method

[e]Wall thickness of the samples estimated by the expression: $P_w = a_0 - P_D$ where $(a_0 = 2d_{100}/\sqrt{3})$

[f]Values obtained from $NH_3$-TPD results

[g]Crystallite size of nickel and platinum oxide calculated from wide angle XRD using Debey–Scherrer equation

[h]Si/Al ratio from ICP-OES analysis

[i]Values obtained by ICP-OES analysis for regenerated Pt/Ni/Al-SBA-15 catalyst

[j]Crystallite size of regenerated Pt/Ni/Al-SBA-15 catalyst using Debey-Scherrer equation from wide angle XRD

Fig. 3a, b. Figure 3a shows the Pt 4f XPS spectra of Pt/Ni/Al-SBA-15 bimetallic catalyst; the binding energies of 71.5 and 74.1 eV have been assigned to $Pt^0$ with respect to Pt $4f_{7/2}$ and Pt $4f_{5/2}$ spin states [21]. The spin state Pt $4f_{5/2}$ corresponding to metallic platinum was clearly observed at 74.1 eV. However, the spin state with respect to metallic Pt $4f_{7/2}$ was not observed, this may be due to the presence of high content of oxidative platinum on this catalyst. In addition, a new peak observed at the binding energy of 73.0 and 77.2 eV were assigned to $Pt^{4+}$ and $Pt^{2+}$ oxidic species [22]. The appearance of this peak indicates that both metallic and oxidative Pt species were present in Pt/Ni/Al-SBA-15 catalyst. The Ni 2p spectrum of bimetallic Pt/Ni/Al-SBA-15 catalyst is shown in Fig. 3b. The two main chemical spin states of Ni $2p_{3/2}$ and Ni $2p_{1/2}$ were observed at binding energy of 854.8 and 873 eV representing the $Ni^{2+}$ state. Further, the two shake up-satellite peaks were found at 860.7 and 879.8 eV, respectively for the emission lines of Ni 2p [23].There was no discernible metallic nickel phase observed in this catalyst, and this confirmed the existence of only NiO. The bulk to surface ratio of Pt and Ni on Pt/Ni/Al/SBA-15 bimetallic catalyst was found to be almost 1:3 corresponding to platinum concentration 0.56% and nickel concentration 1.64% which confirms the dispersion of higher amount of nickel than platinum species over the surface of the catalyst.

### *3.1.4 $NH_3$-TPD acidity measurement*

Figure 4 shows ammonia TPD spectrum of Al-SBA-15 support and Pt, Ni supported mono and bimetallic catalysts. $NH_3$ TPD is one of the efficient techniques to discriminate weak and strong acid sites and to find out their amount and strength. The total acidity values obtained from TPD analysis for support and metal supported catalyst are presented in Table 1. The TPD profiles of Al-SBA-15 exhibited a strong broad peak in the range between 120 to 220 °C, indicating Al atom in the framework and further confirmed the presence of weak and medium acid sites in the Al-SBA-15 support [24]. Pt/Ni/Al-SBA-15 bi-metallic catalyst showed desorption of ammonia in the temperature range of 140–240 °C and 280–340 °C confirming the presence of weak to medium and medium to strong acidic sites on the catalyst. However, on comparing Al-SBA-15 support, Pt/Ni/Al-SBA-15 shows weak, medium and strong acid sites. The bimetallic Pt/Ni-SBA-15 and mono-metallic Pt/SBA-15, Ni/SBA-15 catalyst shows mild acidity that might be due to the presence of surface hydroxyl group attached to the silica matrix. Therefore, the presence of Al on the support could enhance the surface acidity of the Pt/Ni/Al-SBA-15 bimetallic catalyst [25].

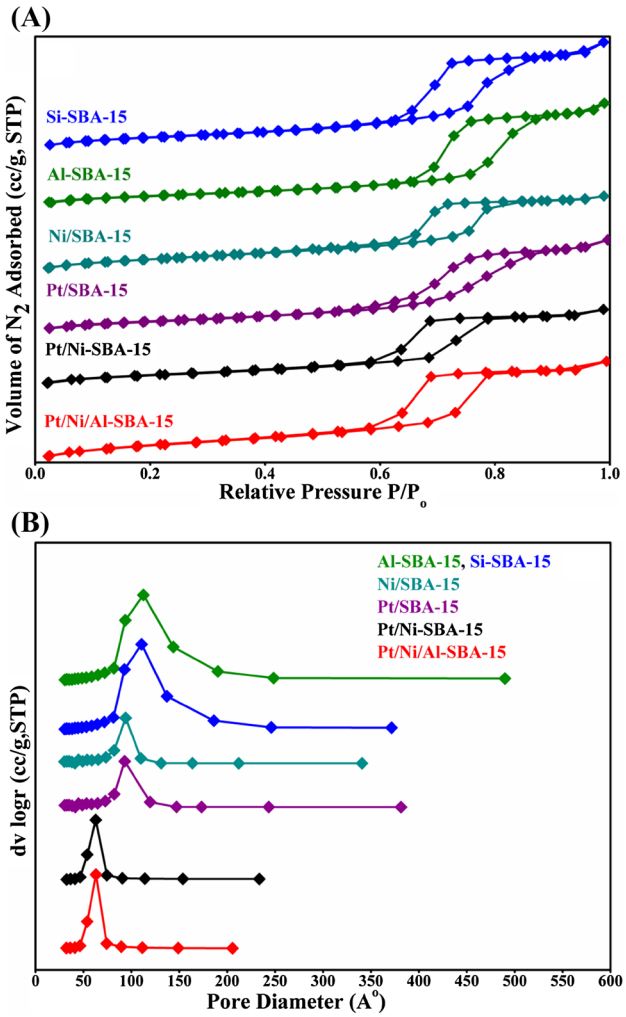


**Fig. 2** **a** Nitrogen sorption isotherms at 77 K for Ni/SBA-15, Pt/SBA-15, Pt/Ni/SBA-15 and Pt/Ni/Al-SBA-15 catalysts. **b** BJH pore size distribution of Ni/SBA-15, Pt/SBA-15, Pt/Ni/SBA-15 and Pt/Ni/Al-SBA-15 catalysts

### *3.1.5 $H_2$-TPR analysis*

The $H_2$-TPR profiles of Pt and Ni supported mono and bimetallic catalyst are shown in Fig. 5. Mono metallic Pt/SBA-15 catalyst showed two different reduction peaks at 111 and 407 °C indicating the existence of $Pt^{2+}$ cations in dispersed as well as bulk state [26]. The hydrogen consumption was maximum observed at low temperature than at higher temperature and this confirmed that most of the $Pt^{2+}$ cations located at 111 °C. Further, it revealed that the dispersed platinum species highly exist at low temperature and which are easily reducible than bulk platinum [27]. In the case of mono metallic Ni/SBA-15 catalyst two distinct reduction peaks in the temperature of 374 and 530 °C were observed. The temperature at 374 °C indicates broad signal, which was related to higher amount of hydrogen that was desorbed than the temperature at 530 °C indicating the strong metal interaction with support. This result suggests that, $Ni^{2+}$ is significantly reduced at 374 °C [19]. On the other hand, by comparing the mono metallic catalyst with bimetallic catalysts the influence of platinum on both acidic and non-acidic supported catalysts can significantly decrease the reduction temperature of $Ni^{2+}/Pt^{2+}$. Bimetallic Pt/Ni-Al-SBA-15 catalyst shows essentially three reduction peaks, the first peak is attributed to the presence of $Pt^{2+}$ at temperature range of 111 °C and it is also to be clearly noted that the second and third reduction temperature of 270 and 320 °C are obtained as a broad signal strongly indicating a possible existence of Ni–Pt species [28], which was favoured by the early reduction of platinum by means of spill over effect [29].

### *3.1.6 HR-TEM analysis*

Figure 6 shows HR-TEM images of mono and bimetal supported mesoporous catalysts; overall the active metal crystallites are well dispersed over the surface of the carrier as can be clearly seen from the images. The original morphology of the support remains intact even after metal loading on the support as evidence from the presence of pores on the support. The nickel and platinum crystallite size in mono metallic catalyst (Fig. 6a, b) shows relatively in the range below 35 nm. However, the majority of these particles were observed at 10–20 nm. Furthermore, the platinum species were uniformly distributed in mono metallic Pt/SBA-15 catalyst, whereas in mono metallic Ni/SBA-15 catalyst shows random distribution of nickel particles. In case of bimetallic Pt/Ni/SBA-15, Pt/Ni/Al-SBA-15 catalysts (Fig. 6c, d), the particle size slightly increased in the range of 35–40 nm on compared with mono metallic catalysts, due to the agglomeration of bimetallic species [30]. However, the majority of reactive bimetallic species was formed in the range of 10–20 nm in Pt/Ni/Al-SBA-15 catalyst and showed uniform distribution. Moreover, the particle size estimated from HR-TEM analysis was well in agreement with crystallite size calculated from high angle XRD as represented in Table 1.

## 3.2 Catalytic hydrodeoxygenation of anisole

### *3.2.1 Effect of Temperature and WHSV*

Figure 7a–d shows the time-on-stream behaviour of anisole conversion for catalyst containing platinum and nickel based mono and bi-metallic catalysts. All tests were performed at two different temperatures 370 and 420 °C and at two different space velocities WHSV ($h^{-1}$) = 3.3 and 6.6. The bimetallic catalysts Pt/Ni/Al-SBA-15 significantly enhanced the conversion of anisole to the desired benzene. On comparing mono and bimetal Pt/Ni supported catalyst; Pt/Ni/Al-SBA-15 shows higher conversion and selectivity. It may

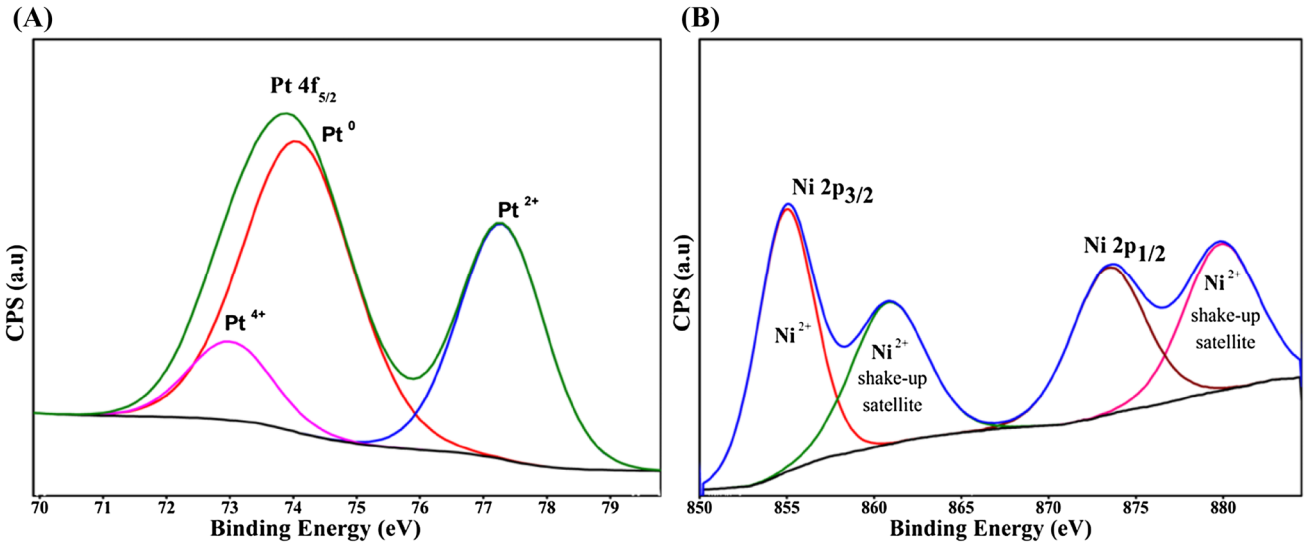


**Fig. 3** XPS spectra of Pt/Ni/Al-SBA-15 catalyst **a** Pt4f contribution, **b** Ni2p contribution

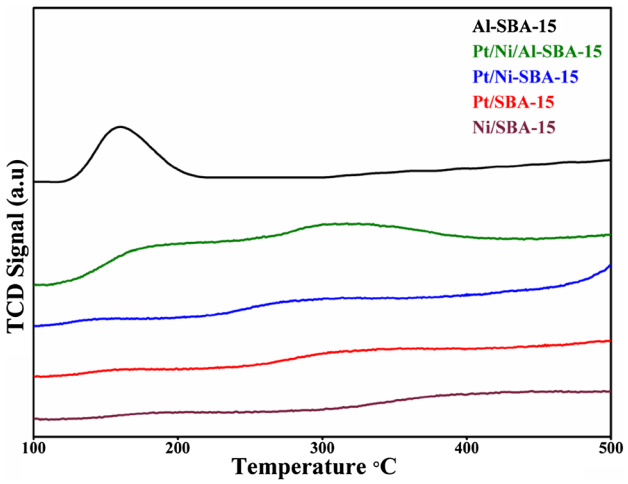


**Fig. 4** $NH_3$-TPD profiles of Al-SBA-15 support and Ni/SBA-15, Pt/SBA-15, Pt/Ni/SBA-15 and Pt/Ni/Al-SBA-15 catalysts

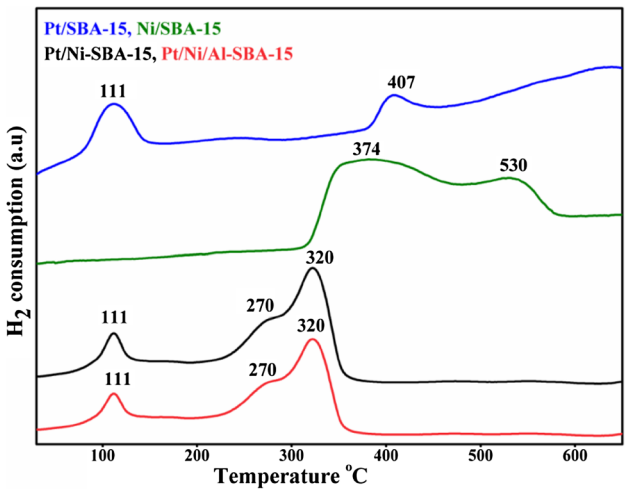


**Fig. 5** $H_2$-TPR profiles of Ni/SBA-15, Pt/SBA-15, Pt/Ni/SBA-15 and Pt/Ni/Al-SBA-15 catalysts

be due to the generation of considerable amount of acidity with high dispersion of Pt/Ni species on the surface of this catalyst. In all cases, the conversion of anisole to benzene and phenol was identified as predominant product and trace amounts of toluene was also observed. Figure 7a, b for Pt/Ni/Al-SBA-15 bimetallic catalyst shows anisole conversion of about 59 and 31% at 420 °C with respect to lower and higher WHSV respectively, whereas, at lower temperature of 370 °C (Fig. 7c, d) it showed 31 and 26% of anisole conversion. The optimum conversion was observed at 420 °C with respect to lower space velocity. On comparison with bimetallic catalyst Pt/Ni /SBA-15, at 420 °C anisole conversion of about 45 and 23% for lower WHSV and higher WHSV were obtained. However, at 370 °C, 21 and 19% were obtained. In the present experimental conditions, mono metallic Pt/SBA-15 (Fig. 7a, b) showed relatively low conversion, with the maximum conversion of about 3% at 420 °C, under lower WHSV. Further increasing of the WHSV there is no considerable changes observed, which may be due to the moderate capacity of hydrogenolysis of C–O bond in the anisole. However, its benzene selectivity is excellent than other catalysts studied. These results suggest that hydrogenolysis of phenolic C–O bond occurs effectively than subsequent demethylation and methyl transfer at higher temperature. However, the mono metallic Ni/SBA-15 performed fairly higher compared to Pt/SBA-15 with maximum conversion 20 and 8% at temperature of about 420 °C with lower and higher WHSVs ($h^{-1}$) of 3.3 and 6.6. These results further

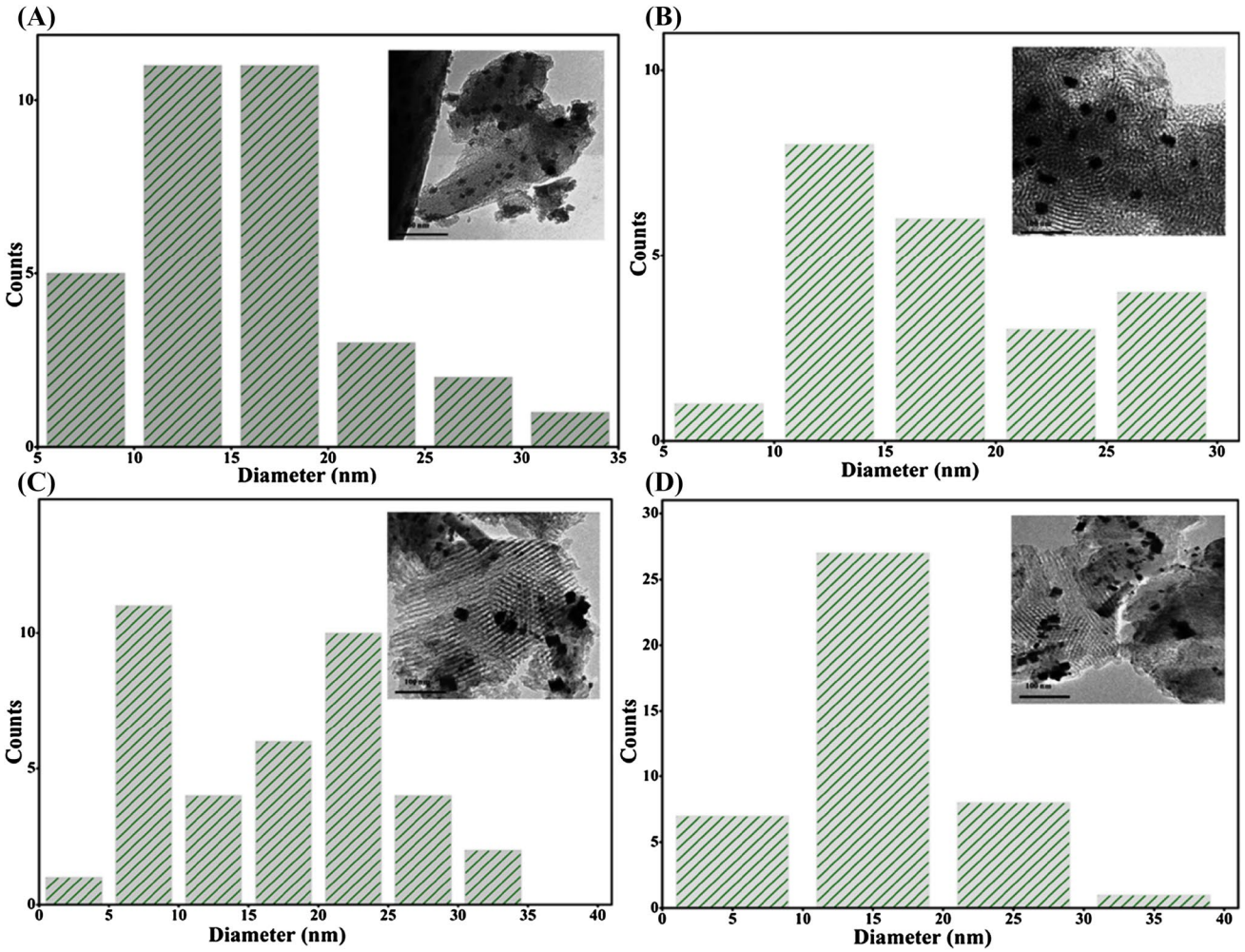


**Fig. 6** HR-TEM images and particle size distribution of oxide catalyst **a** Ni/SBA-15, **b** Pt/SBA-15, **c** Pt/Ni/SBA-15, **d** Pt/Ni/Al-SBA-15

suggested that acidic bimetallic catalyst Pt/Ni/Al-SBA-15 showed better conversion and product selectivity towards benzene formation under the present experimental condition. And, it clearly arises due to the relative favourable synergetic catalytic effect that exist between metal and acid sites [31, 32].

### *3.2.2 Effect of WHSV over Product distribution*

The time-on-stream behaviour with respect to product selectivity towards anisole hydrotreating over bimetallic and mono metallic catalysts at two different WHSV and temperature of 420 °C are presented in (Fig. 8a–h). The maximum conversion and benzene selectivity were observed for all the catalysts at 420 °C. At lower WHSV ($h^{-1}$) of 3.3 with the temperature of 420 °C, Pt/Ni/Al-SBA-15 bimetallic catalyst (Fig. 8a, b) showed product distribution towards benzene selectivity of about 36%, whereas, at higher WHSV ($h^{-1}$) showed 37% of benzene selectivity. On increasing the space velocity, the formation of benzene was slightly increased and further toluene formation also observed to maximum of 3% at 420 °C. The bimetallic Pt/Ni-SBA-15 catalyst operating at reaction temperature of 420 °C with lower WHSV ($h^{-1}$) 3.3 (Fig. 8c) shows the maximum benzene selectivity of 22%. However, increasing the WHSV ($h^{-1}$) to 6.6 (Fig. 8d), it showed 31%. About 2% of toluene was observed at lower WHSV and at higher WHSV toluene formation was not observed. The product selectivity with respect to mono metallic Ni/SBA-15 (Fig. 8e, f) showed maximum benzene selectivity of 31% at lower WHSV ($h^{-1}$) 3.3, whereas at higher WHSV ($h^{-1}$) 6.6 it showed 11% at 420 °C. The mono metallic Ni/SBA-15 catalyst revealed that on increasing the WHSV, it could not increase the product formation of benzene. However, mono metallic platinum and bimetallic catalysts could enhance the product formation of benzene at higher WHSV. In general, the conversion with respect to all the catalysts showed maximum at lower WHSV than at higher WHSV.

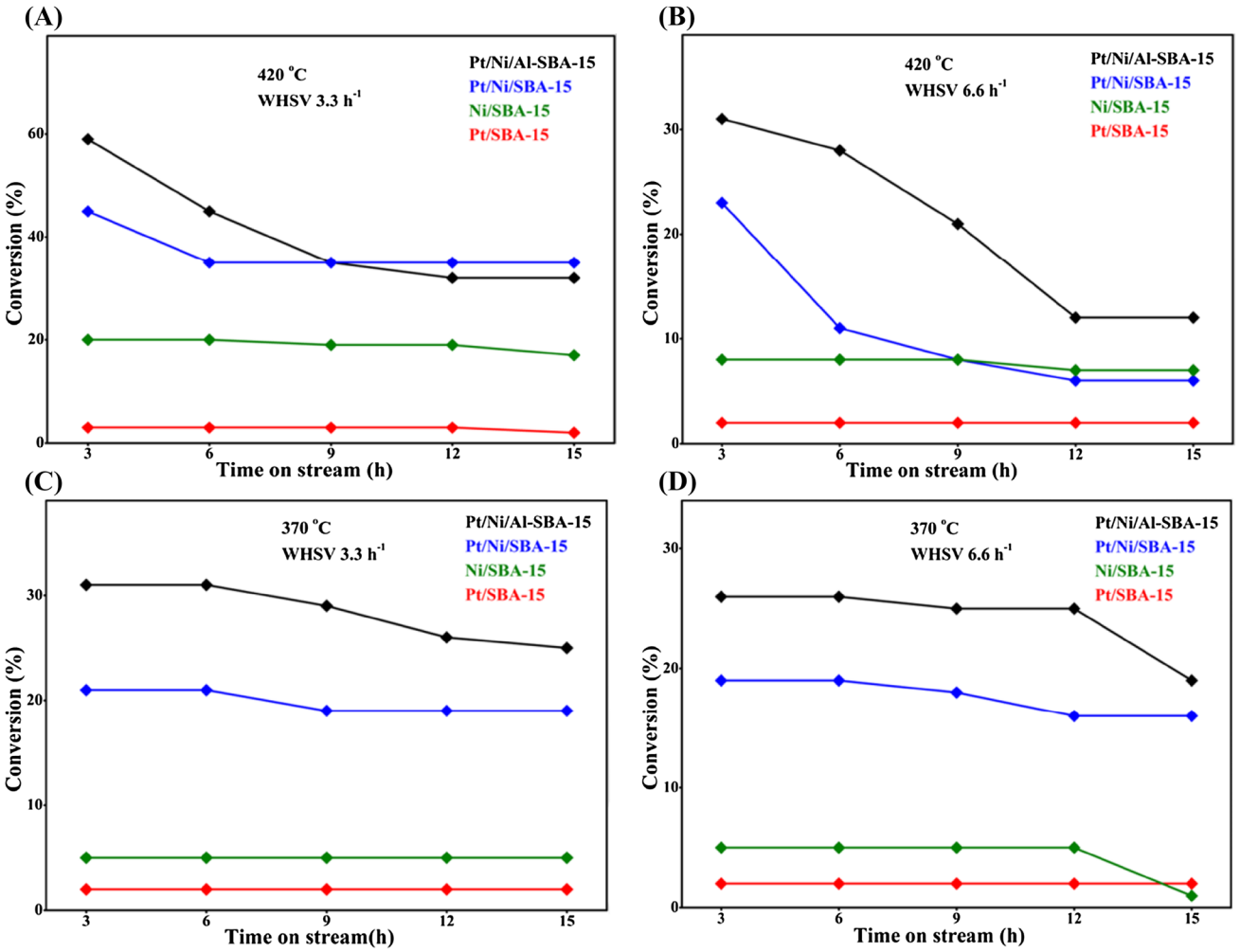


**Fig. 7** **a–d** Anisole conversions with respect to different weight hourly space velocity for Pt/Ni/Al-SBA-15, Pt/Ni/SBA-15, Pt/SBA- 15 and Ni/SBA-15 catalysts at 370 and 420 °C. Conditions: WHSV ($h^{-1}$) = 3.3, 6.6; temperature = 370 and 420 °C; $H_2$ = 50 mL $min^{-1}$

The time-on-stream behaviour and product selectivity of mono metallic platinum catalyst are shown in (Fig. 8g, h) at specified reaction condition. The platinum based mono metallic catalyst showed 35% benzene selectivity at 420 °C under lower space velocity, however at higher space velocity 55% was observed. The maximum benzene selectivity was observed for this catalyst, which may be due to the presence of uniform dispersion of active platinum on the external surface of the support as seen from HR-TEM images. In addition to that after formation of phenol intermediate, hydrogenolysis takes place more rapidly to produce benzene than subsequent process. However, this catalyst shows much lower conversion than other catalysts studied, possibly this may be due to the existence of strong interaction between anisole molecule and metal surface leading to higher coke formation at a higher temperature.

According to the activity results, the supports seem to have significant influence on selectivity of benzene. However, the acidic nature of bimetallic Pt/Ni/Al-SBA-15 showed higher conversion and selectivity than mono and other bimetallic catalysts. The acidic Al-SBA-15 support has significant effect on benzene and toluene selectivity than Si-SBA-15 support. The best catalytic response of the bimetallic Pt/Ni/Al-SBA-15 catalyst in hydrodeoxygenation of anisole could be explained by considering the combination of various effects. One of them being the largest surface exposure of the active phase as determined by HR-TEM, presenting active phases well dispersed on external catalyst surfaces. Also, the Pt/Ni/Al-SBA-15 catalyst records the maximum total acidity among the catalyst studied (Table 1). Considering a correlation between acid sites and metallic sites for catalytic activity of anisole, the major activity of Pt/Ni/Al-SBA-15 could be explained by cleavage of methyl carbon–oxygen bond, which might occur on both metal and acid sites of the catalyst. These results suggests that the presence of acidity and the better dispersion of active metal

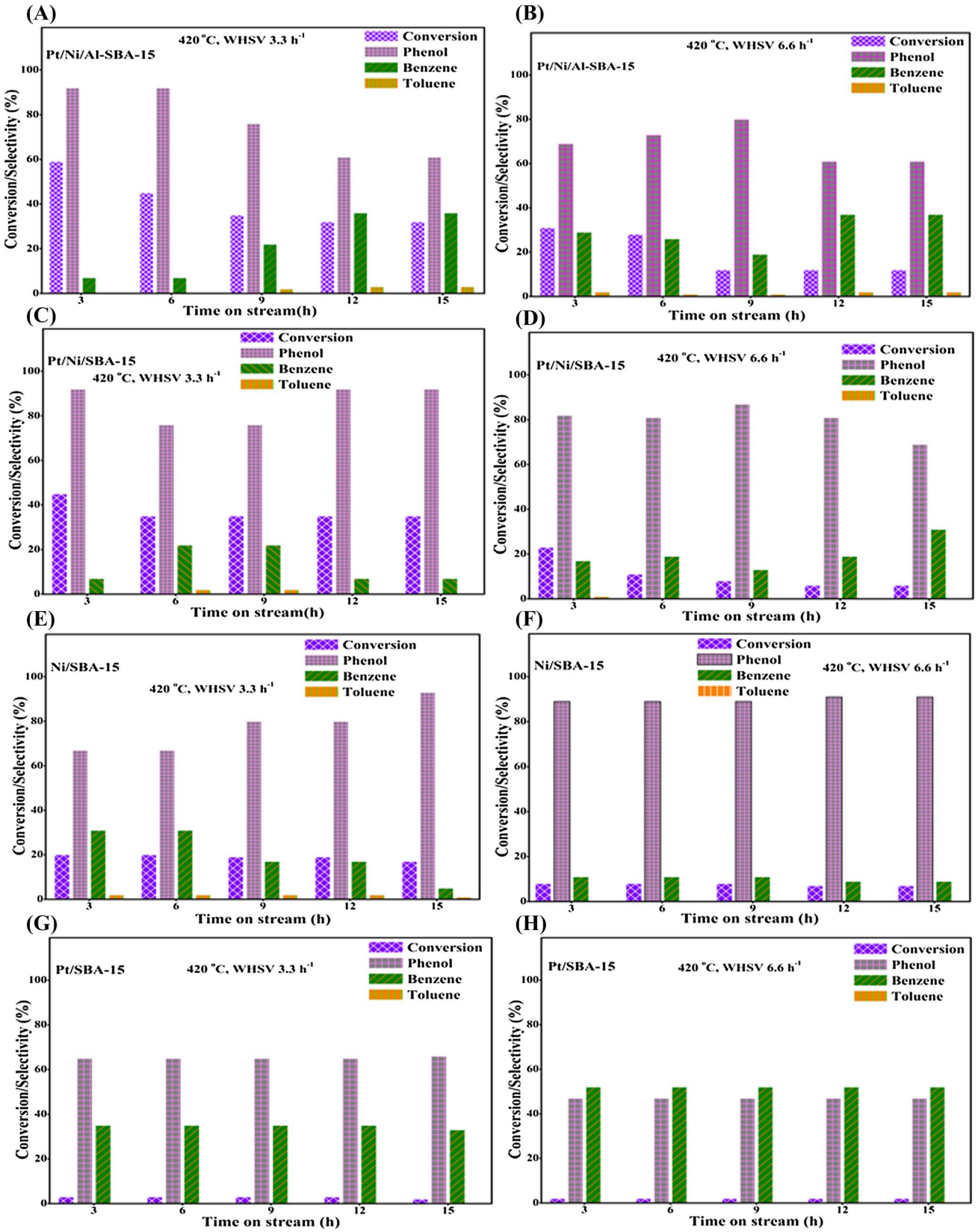


**Fig. 8** **a–h** Anisole conversion and product selectivity over Pt/Ni/Al-SBA-15, Pt/Ni/SBA-15, Pt/SBA-15, and Ni/SBA-15 catalysts at 420 °C with respect to different weight hourly space velocity. Conditions: WHSV ($h^{-1}$) = 3.3, 6.6; temperature = 420 °C; $H_2$ = 50 mL $min^{-1}$

could improve its activity for HDO and further modification of the support may also be contributing to the reaction conversion by changing the binding strength of reactive species on the support surface through interaction between nickel and platinum. This effect has also been identified in other catalytic studies of hydrocarbon hydrogenation reactions [33]. The higher conversion of Pt/Ni/Al-SBA-15 bimetallic catalyst may be due to the presence of large synergistic effect between metal and acid sites and further addition of platinum to nickel could enhance the reducibility of nickel, which utilizes the more molecular hydrogen into atomic hydrogen for cleavage of C–O bond via hydrogenolysis process.

### *3.2.3 Possible reaction pathways in HDO of anisole*

Concerning the mechanisms by which anisole may undergo HDO reaction, previous investigations have suggested that there are two main parallel pathways [34]. Figure 9 represents conversion pathway of anisole, path way (a) HDO route leading to form phenol intermediate via cleavage of methoxy C–O bond followed by elimination of $CH_4$ and subsequent hydrogenolysis of phenolic C–O bond leading to form benzene and further hydrogenation of aromatic ring was restricted as confirmed from GC analysis of the reaction products. Path way (b) trans-methylation was another class of reaction; in this class of reaction methyl phenol was identified as intermediate and followed by hydrogenolysis of phenolic C–O bond of this intermediate produces toluene [13, 35, 36].

Pathway (d) represents direct deoxygenating route of aromatic ring, which was restricted, as confirmed from the absence of methanol from GC analysis and further ring hydrogenated product was not identified. The trans-methylated product of toluene maximum 3% was identified in Pt/Ni/Al-SBA-15 catalyst, and it confirmed that the acidic site on the catalyst may favour the trans-methylation path. However, the Pathway (a) was identified as the predominant route for all the catalyst studied. Furthermore, on the basis of reaction pathway, the ratio of (benzene:toluene) was calculated for Pt/Ni/Al-SBA-15 bimetallic catalyst under the optimum reaction condition of 420 °C with WHSV ($h^{-1}$) = 3.3, the ratio of benzene to toluene showed (1:0.08), and it confirmed that the formation of benzene pathway was predominant than the toluene pathway. Nevertheless, the concentration of benzene was achieved as maximum compared with toluene and this suggests that the catalyst predominantly works through demethylation path way. Therefore, the demethylation pathway was identified more significant than other subsequent pathways.

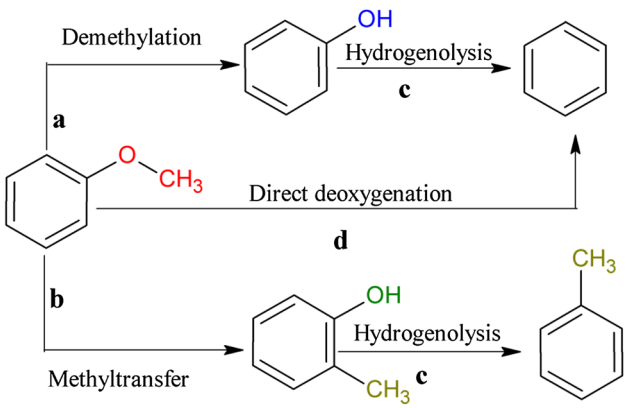


**Fig. 9** The plausible routes for anisole hydrotreating

### *3.2.4 Catalyst deactivation study*

Sintering and coke deposition are the main factor for deactivation of catalysts. The deactivation behaviour of mono and bimetallic catalysts was studied after anisole hydrotreating at 420 °C. Figure 10 shows the thermal gravimetric analysis of spent catalysts after reaction at 420 °C with space velocity 3.3 $h^{-1}$ on 15 h on-stream. The thermogram shows the following increasing order for the formation of coke in the catalyst 4.0% < 6.5% < 8.0% < 9.5% for Pt/Ni/Al-SBA-15, Pt/Ni/SBA-15, Ni/SBA-15 and Pt/SBA-15 respectively. In general, the formation of coke on the bimetallic catalyst was resisted more than the mono-metallic catalysts. This might be due to the large surface synergistic effect of the Pt with Ni over Al-SBA-15, which was similarly observed and reported in the literature [37]. The major coke content observed at 340 °C indicates that the catalytic performance in terms of conversion was suppressed due to the formation of coke. However, some weight loss also occurred due to the moisture produced as by-product on the catalyst surface which may hinder the activity of the catalyst. After regeneration,

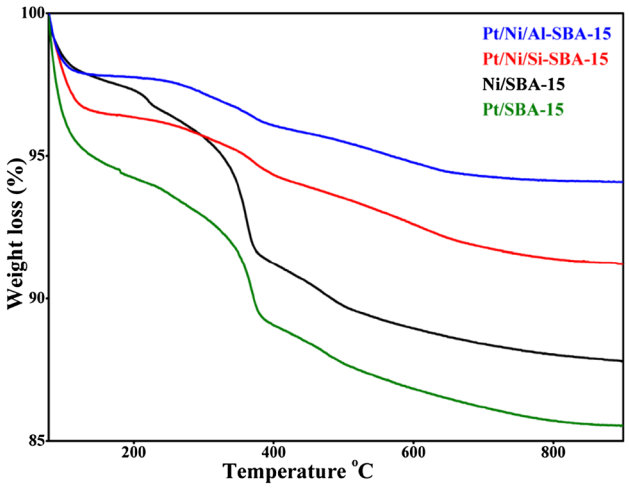


**Fig. 10** Thermal gravimetric analysis of spent Ni/SBA-15, Pt/SBA-15, Pt/Ni/SBA-15 and Pt/Ni/Al-SBA-15 catalysts

the particle size estimated from high angle XRD for Pt/Ni/Al/SBA-15 catalyst was accounted to be 21 and 16 nm with respect to nickel and platinum oxide respectively. The particle size was not much altered before and after regeneration in the thermal treatment as shown in Table 1. It demonstrates that the sintering may not be responsible for catalyst deactivation since the reaction temperature of 420 °C is extensively lower than the melting point of nickel and platinum. The inhibition of catalytic activity was mainly due to coke formation and not sintering. The conversion and selectivity with respect to optimized Pt/Ni/Al-SBA-15 bimetallic catalyst was studied under condition of 420 °C with WHSV of 3.3 $h^{-1}$ and the results were represented in Fig. 11. The maximum anisole conversion 58% with benzene selectivity 38% was observed. The reuse experiment demonstrates that the catalytic activity could not vary significantly with relevant to its fresh catalytic run. Even though, a small variation in the product distribution was occurred, this may be due to the redistribution of active Pt/Ni species by the thermal treatment in the regeneration of catalyst. Furthermore, the loss of metal content after reaction was analysed by ICP-OES technique, the metal loss in the bimetallic catalyst Pt/Ni/Al-SBA-15 was found to be insignificant, which was further confirmed by the retention of catalytic activity after regeneration as shown in Fig. 11. The study clearly shows that Pt/Ni/Al-SBA-15 bimetallic catalyst provided high HDO yield exhibiting higher anisole conversion of 59% combined with benzene selectivity of 37% under atmospheric pressure. Ni/Pt sites show superior ability for adsorbing and activating $H_2$ could facilitate the transformation of anisole to hydrocarbon via HDO. Moreover, the main results from this study was that the acidic features of this catalyst arising from the Al-SBA-15 support could enhance the interaction with the anisole molecules, causing their adsorption through acidic and metallic sites favouring their transformation through C–O bond cleavage via demethylation and hydrogenolysis pathways to produce hydrodeoxygenated aromatics.

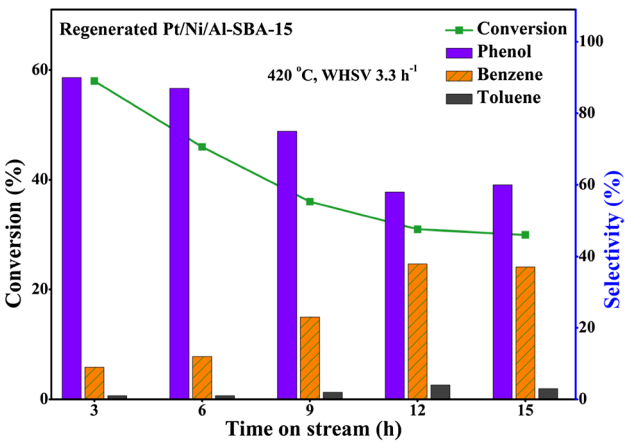


**Fig. 11** Anisole conversion and product selectivity for regenerated Pt/Ni/Al-SBA-15 catalyst at 420 °C. Conditions: WHSV ($h^{-1}$) = 3.3; temperature = 420 °C; $H_2$ = 50 mL $min^{-1}$

## 4 Conclusions

The nickel and platinum based supported catalysts have been developed heterogeneously and evaluated in HDO of anisole, Pt/Ni/Al-SBA-15 bimetallic catalyst were found to be more attractive for the HDO than single site Pt and Ni catalysts. However, Pt facilitates nickel oxide reduction at temperature lower than 350 °C by spillover effect. The acidic support of Al-SBA-15 was more relevant in the conversion and benzene selectivity, which additionally enhanced the activation of anisole on the catalyst surface than non acidic support of Si-SBA-15. The high catalytic performance of Pt/Ni/Al-SBA-15 was attributed to the unique characteristic of acidic Al-SBA-15 support and further to the high dispersion of platinum and nickel particles over the external surface of the support and also to the possible synergistic effect that exists in this catalyst. The presence of strong metal support interaction and differences in the active phase distribution may lead to lower anisole conversion on mono metallic catalyst. However, on comparing the activity of mono and bimetallic catalytic system, the bimetallic catalyst gave more HDO yield.

**Acknowledgements** The author acknowledges UGC-BSR (603/PD6/2007) New Delhi, India for the awarding of Research Fellowship. The facilities provided by DST-FIST (SR/S5/NM-35/2005) and UGC-DRS are gratefully acknowledged.

## References

1. G.W. Huber, S. Iborra, A. Corma, Chem. Rev. **106**, 4044 (2006)
2. S. Pichaikaran, P. Arumugam, Green Chem. **18**, 2888 (2016)
3. W. Keim, Pet. Chem. **50**, 298 (2010)
4. Q. Meng, H. Fan, H. Liu, H. Zhou, Z. He, Z. Jiang, ChemCatChem. **7**, 2831 (2015)
5. T.M. Sankaranarayanan, A. Berenguer, C. Ochoa-hernández, I. Moreno, P. Jana, J.M. Coronado, D.P. Serrano, P. Pizarro, Catal. Today **243**, 163 (2015)
6. T.V. Choudhary, C.B. Phillips, Appl. Catal. A, Gen. **397**, 1 (2011)
7. A. Berenguer, T.M. Sankaranarayanan, G. Gómez, I. Moreno, J.M. Coronado, P. Pizarro, D.P. Serrano, Catal. Today **243**, 163 (2015)
8. P.M. Mortensen, J. Grunwaldt, P.A. Jensen, K.G. Knudsen, A.D. Jensen, Appl. Catal. A, Gen. **407**, 1 (2011)
9. N. Yan, Y. Yuan, R. Dykeman, Y. Kou, P.J. Dyson, Angew. Chemie - Int. Ed. **49**, 5549 (2010)
10. X. Zhu, L.L. Lobban, R.G. Mallinson, D.E. Resasco, J. Catal. **281**, 21 (2011)
11. Z. He, X. Wang, Catal. Sustain. Energy **1**,28 (2012)
12. K. Barbera, P. Lanzafame, A. Pistone, S. Millesi, G. Malandrino, A. Gulino, S. Perathoner, G. Centi, J. Catal. **323**, 19 (2015)
13. O. Shea, Y. Yang, C. Ochoa-hernández, V.A. De, P. Pizarro, J.M. Coronado, D.P. Serrano, Appl. Catal. B Environ. **145**, 91 (2014)

14. V.A. Yakovlev, S.A. Khromova, O.V. Sherstyuk, V.O. Dundich, D.Y. Ermakov, V.M. Novopashina, M.Y. Lebedev, O. Bulavchenko, V.N. Parmon, Catal. Today **144**, 362 (2009)
15. M. Saidi, F. Samimi, D. Karimipourfard, T. Nimmanwudipong, B.C. Gates, M.R. Rahimpour, Energy Environ. Sci. **7**, 103 (2014)
16. A. Vinu, B.M. Devassy, S.B. Halligudi, W. Böhlmann, M. Hartmann, Appl. Catal. A, Gen. **281**, 207 (2005)
17. Y. Yue, A. Gédéon, J. Bonardet, N. Melosh, J.D. Espinose, Chem. Commun. (Camb). **19**, 1967 (1999)
18. W. Chen, Z. Luo, C. Yu, Y. Yang, G. Li, J. Zhang, Fuel Process. Technol. **126**, 420 (2014)
19. M. Lindo, A.J. Vizcaíno, J.A. Calles, A. Carrero, Int. J. Hydrogen Energy **35**, 5895 (2010)
20. K.V.R. Chary, C.S. Srikanth, Catal. Lett. **128**, 164 (2009)
21. X. Fan, J. Li, Z. Zhao, Y. Wei, J. Liu, A. Duan, G. Jiang, RSC Adv. **5**, 28305 (2015)
22. D.J. Kim, J.W. Kim, S.J. Choung, M. Kang, J. Ind. Eng. Chem. **14**, 308 (2008)
23. L. Pandolfi, P. Cafarelli, S. Kaciulis, A.A.G. Tomlinson, Microporous Mesoporous Mater. **110**, 64 (2008)
24. X. Zheng, B. Dong, C. Yuan, J. Porous Mater. **20**, 539 (2012)
25. V. Sundaramurthy, I. Eswaramoorthi, A.K. Dalai, J. Adjaye, Microporous Mesoporous Mater. **111**, 560 (2008)
26. I. Sobczak, M. Ziolek, M. Nowacka, Microporous Mesoporous Mater. **78**, 103 (2005)
27. S. Shen, S. Kawi, Appl. Catal. B Environ. **45**, 63 (2003)
28. J. Arenas-Alatorre, A. Gómez-Cortés, M. Avalos-Borja, G. Díaz, J. Phys. Chem. B **109**, 2371 (2005)
29. F.V. Barsi, D. Cardoso, Brazilian J. Chem. Eng. **26**, 353 (2009)
30. C. Wang, L. Zhang, Y. Liu, Appl. Catal. B Environ. **136–137**, 48 (2013)
31. A.J. Foster, P.T. Do, R.F. Lobo, Top. Catal. **55**, 118 (2012)
32. R.C. Runnebaum, T. Nimmanwudipong, R.R. Limbo, D.E. Block, B.C. Gates, Catal. Lett. **142**, 7 (2012)
33. A.M. Venezia, V. La Parola, B. Pawelec, J.L.G. Fierro, Appl. Catal. A, Gen. **264**, 43 (2004)
34. J.E. Peters, J.R. Carpenter, D.C. Dayton, Energy & Fuels **29**, 909 (2015)
35. C.V. Loricera, B. Pawelec, A. Infantes-molina, M. C. Álvarez-galván, Catal. Today **172**, 103 (2011)
36. W. Lee, Z. Wang, R.J. Wu, A. Bhan, J. Catal. **319**, 44 (2014)
37. J. Feng, M. Zhang, Y. Yang, Chin. J. Chem. Eng. **22**, 1232 (2014)